This document is confidential and is proprietary to the American Chemical Society and its authors. Do not copy or disclose without written permission. If you have received this item in error, notify the sender and delete all copies.

Reversible self-assembly of water soluble gold(I) complexes

Journal:	*Inorganic Chemistry*
Manuscript ID	ic-2017-023432.R1
Manuscript Type:	Article
Date Submitted by the Author:	n/a
Complete List of Authors:	Aguiló, Elisabet; Universitat de Barcelona, Inorganic Department Moro, Artur; FCT, Universidade Nova de Lisboa, REQUIMTE - Departamento de Química Gavara, Raquel; Universitat de Barcelona, Departament de Química Inorgànica Alfonso, Ignacio; Instituto de Quimica Avanzada de Cataluña (IQAC), Quimica Biologica y Modelizacion Molecular Perez, Yolanda; Institute of Advanced Chemistry of Catalonia, Servicio de Resonancia Magnética Nuclear Zaccaria, Francesco; Vrije Universiteit Amsterdam Fonseca Guerra, Celia; Vrije Universiteit Amsterdam, Department of Theoretical Chemistry Malfois, Marc; ALBA Synchrotron Light Laboratory (CELLS) Baucells, Clara; Universitat de Barcelona, Inorganic Department Ferrer, Montserrat; Universitat de Barcelona, Quimica Inorganica Lima, João; REQUIMTE, Univ. Nova de Lisboa, Chemistry Rodríguez, Laura; Universitat de Barcelona, Ìnorganic and Organic Chemistry

SCHOLARONE™
Manuscripts

Reversible self-assembly of water soluble gold(I) complexes

Elisabet Aguiló,[a] Artur J. Moro,[b] Raquel Gavara,[a] Ignacio Alfonso,[c] Yolanda Pérez,[d] Francesco Zaccaria,[e] Célia Fonseca Guerra,[e,f] Marc Malfois,[g] Clara Baucells,[a] Montserrat Ferrer,[a] João Carlos Lima[b,*] and Laura Rodríguez.[a,h*]

[a] *Departament de Química Inorgànica i Orgànica. Secció de Química Inorgànica. Universitat de Barcelona, Martí i Franquès 1-11, 08028 Barcelona, Spain. Tel.: +34 934039130. e-mail: laura.rodriguez@qi.ub.es*

[b] *LAQV-REQUIMTE, Departamento de Química, CQFB, Universidade Nova de Lisboa, Monte de Caparica, Portugal. e-mail: lima@fct.unl.pt*

[c] *Departamento de Química Biológica y Modelización Molecular, IQAC–CSIC, Jordi Girona, 16-26, E-08034 Barcelona, Spain*

[d] *NMR-Facility, IQAC–CSIC, Jordi Girona, 16-26, E-08034 Barcelona, Spain*

[e] *Department of Theoretical Chemistry, Amsterdam Center for Multiscale Modeling (ACMM), VU Amsterdam, The Netherlands.*

[f] *Leiden Institute of Chemistry, Gorlaeus Laboratories, Leiden University, The Netherlands*

[g] *ALBA Synchrotron Light Laboratory (CELLS). Carrer de la Llum 2-26. 08290 Cerdanyola del Vallès – Barcelona, Spain*

[h] *Institut de Nanociència i Nanotecnologia (IN^{2}UB). Universitat de Barcelona, 08028 Barcelona (Spain)*

Abstract

The reaction of the gold polymers containing bipyridyl and terpyridyl units, $[Au(C{\equiv}C\text{-}C_{15}H_{10}N_3)]_n$ and $[Au(C{\equiv}C\text{-}C_{10}H_7N_2)]_n$, with the water soluble phosphines PTA and DAPTA gives rise to the formation of four gold(I) alkynyl complexes that self-assemble in water and in DMSO, through different intermolecular interactions, with impact on the observed luminescence displayed by the supramolecular assemblies.

A detailed analysis carried out by NMR studies performed in different DMSO:D_2O mixtures indicates the presence of two different assembly modes in the aggregates: (i) chain assemblies that are based mainly on aurophilic interactions and (ii) stacked assemblies which are based on Au···π and π···π interactions. These different supramolecular environments can be also detected by their intrinsic optical properties (differences in absorption and emission spectra) and are predicted by the changes in relative binding energy from DFT theoretical calculations carried out in DMSO and water. SAXS experiments performed in the same mixture of solvents are in agreement with the formation of aggregates in all cases.

The aromatic units chosen, bipyridine and terpyridine, allow the use of external stimuli to reversibly change the aggregation state of the supramolecular assemblies. The interaction with Zn^{2+} cation is observed to disassemble the aggregates, while encapsulating agents competing for Zn^{2+} complexation revert the process to the aggregation stage, as verified by SAXS and NMR. The adaptive nature of the supramolecular assemblies to the metal ion content is accompanied by significant changes in the absorption and emission spectra, signaling the aggregation state and also the content on Zn^{2+}.

Keywords: gold(I); aggregation; reversible systems; NMR; SAXS; DFT; self-assembly

Introduction

Self-assembly of small molecules by the establishment of non-covalent interactions has received great attention in the past decade as a way to build supramolecular structures with a large number of specific functions and morphologies.[1-4] As a result, supramolecular chemistry has matured from a conceptually marvellous scientific curiosity to a technologically relevant science encompassing a broad area of advanced materials.[5] Within this field, gold(I) complexes represent an emerging area of investigation in the last years, as they show weak Au(I)···Au(I) interactions which can modulate and govern the resulting assemblies and properties in very different potential applications.[6,7] It was recently shown that small molecules of the type R-Au(I)-alkynylpyridine, where R is a water soluble phosphine (compounds **A** and **B** in Chart 1), self-assemble to form long fibers and hydrogels through intermolecular π stacking and metallophilic interactions.[8,9] Replacing the pyridine moiety by a different aromatic unit such as coumarin (compound **C**, in Chart 1) does not hamper the assembling ability of these molecules.[10] On the other hand, the introduction of a positive charge on the chemical structure either at the phosphine (complexes **1** and **4** Chart 1) or at the pyridyl unit (complexes **2**, **3**, **5** and **6**) switches the fibrillary self-assembly into rods, spherical vesicles or square-like morphologies.[11]

Novel supramolecular nanostructures constituted by the non-covalent self-organization of small metallophilic molecules with tunable properties are underexplored within the field of self-assembling materials. A research interest has increased in the last years in the construction of stimuli-responsive metallosupramolecular architectures with diverse sizes, shapes, and symmetries due to their promising applications such as molecular transporting devices, chemosensors, optoelectronic devices, drug delivery, tissue engineering, biomaterials, surface science, displays, etc.[5,12-16] Stimuli-responsive systems are capable to modulate their behavior in a differential manner depending on the external stimulus to which they are exposed, being a considerable challenge for supramolecular chemists.

The modular chemistry of Au(I)-alkynyl complexes furthermore allows for a rational design where solubility and function can be added to program supramolecular assembly into nanostructures which can be tuned by changes in charge or polarity, among others.

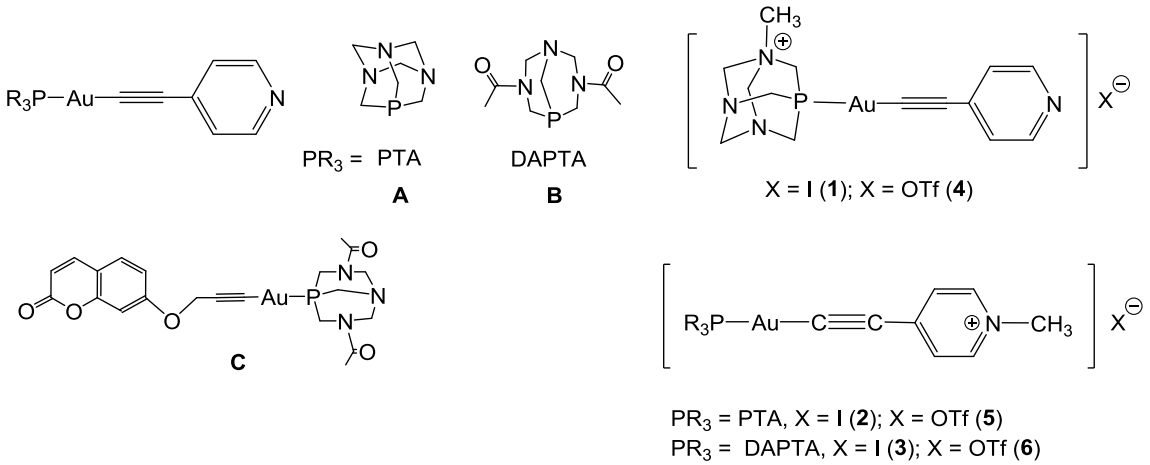

Chart 1. Molecular structures of the gold(I)-alkynyl complexes previously studied.

In this work we extend the development of these small molecules by adding a chelating unit able to trigger the assembly/disassembly process by external stimuli (e.g. cations and chelating molecules). At the same time, the increase in the number of aromatic rings, will allow a change in the balance between Au···Au and π···π interactions, which will impact on the stability of the aggregates. The complexation with cations will significantly change the electrostatic balance of the assemblies leading to dissociation. The disassembly can be reversed by the addition of molecules that compete for the metal cation, leading to reassemble of the nanostructures.

Experimental Section

General procedures

All manipulations have been performed under prepurified N_2 using standard Schlenk techniques. All solvents have been distilled from appropriated drying agents. Commercial reagents 1,3,5-triaza-7-phosphatricyclo[3.3.1.13.7]decane (PTA, Aldrich 97%), 3,7-diacetyl-1,3,7-triaza-5-phosphabicyclo[3.3.1]nonane (DAPTA, Aldrich 97%) have been used as received. Literature methods have been used to prepare 5-ethynyl-2,2'-bipyridine,[17] 4'-ethynyl-2,2'-6',2''-terpyridine,[18] $[Au(C\equiv C\text{-}C_{15}H_{10}N_3)]_n$[19] and $[Au(C\equiv C\text{-}C_{10}H_7N_2)]_n$.[20]

Physical measurements

Infrared spectra have been recorded on a FT-IR 520 Nicolet Spectrophotometer. ^{1}H-NMR (δ(TMS) = 0.0 ppm), $^{31}P\{^1H\}$-NMR (δ(85% H_3PO_4) = 0.0 ppm) spectra have been obtained on a Varian Mercury 400 and Bruker 400. One- and two-dimensional (1D and 2D) NMR experiments were performed also at 298 K on a 500 MHz Bruker AVANCEIII-HD equipped with a z-gradient (65.7 G cm^{-1}) inverse TCI-cryoprobe. The gradient strength was calibrated using the diffusion coefficient of water in a standard solution of 0.1 mg/ml $GdCl_3$, 0.1% DSS, 1% H_2O in D_2O. **2a** and **2b** samples were dissolved in the corresponding deuterated solvent containing 3-(trimethylsilyl) propionic-2,2,3,3-d_4 -acid sodium salt (TSP-d_4). TSP-d_4 was used as an internal standard both for calibrating the ^{1}H and ^{13}C chemical shifts and for estimating the relative concentration changes upon aggregation. Bruker TopSspin 3.5pl6 standard pulse sequences were used for 1D and 2D experiments. To obtain the highest receiver gain and to apply the minimum amount of scans and increments using low sample concentrations ($\leq$ 1 mM), the reduction of residual water in the NMR spectra (coming from the sample and/or on deuterated solvents) was needed, so pulse sequences with a soft suppression of the water resonance were used. 1D ^{1}H experiments were acquired using the zgesgppe pulse sequence, which incorporates water suppression using excitation sculpting with gradients and perfect echo. For 2D ^{1}H-^{1}H experiments, excitation sculpting for ^{1}H-^{1}H NOESY (noesyesgpph pulse program) and 3-9-19 pulse train for DOSY (stebpgp1s19 pulse program) were applied for water suppression. 2D ^{1}H-^{13}C (HSQC and HMBC) experiments were also acquired. Spin-lattice (T_1) and spin-spin (T_2) relaxation times were measured for

2b complex using standard inversion-recovery pulse sequence for T_1 and PROJECT-CPMG[21] for T_2.

2D DOSY[22] experiments were performed using a stimulated-echo sequence incorporating bipolar gradient pulses and one spoil gradient. The gradient strength was logarithmically incremented in 18-24 steps from 5 to 98% of its maximum value. Diffusion times and gradient pulse durations were optimized for each experiment. Typically, diffusion times between 60 and 120 ms and bipolar rectangular gradient pulses between 2.0 ms were employed. Diffusion NMR data were processed and represented using the free software DOSY Toolbox.[23] The translational diffusion coefficient obtained for different samples was used to estimate the "apparent" size of the gold(I) complexes in different solvent composition. For the calculation of the hydrodynamic radii, the diffusion coefficients were obtained from the monoexponential fitting of the integral values versus gradient strength using the Topspin 3.5pl6 Relaxation module. When calculating and interpreting the hydrodynamic radii values, we have taken into account two facts: 1) the Stokes-Einstein equation is only valid for spherical particles with sizes larger that the solvent molecules; 2) the effects of chemical exchange in diffusion spectra.[22] In our case, for DMSO-d_6 and DMSO-d_6 with low amounts of D_2O, we expected to have mainly monomer or dimers molecules in solutions, so our gold(I) complexes have a slightly larger size than solvent. Therefore, for our r_H calculations, we followed the method described by Macchioni et al.,[24] using the expression of factor c as a function of r_{solv}/r_H was derived by Chen et al.[25] and the approximation that our complexes were spherical.

ElectroSpray-Mass spectra (+) have been recorded on a Fisons VG Quatro spectrometer. Absorption spectra have been recorded on a Varian Cary 100 Bio UV- spectrophotometer and emission spectra on a Horiba-Jobin-Ybon SPEX Fluorolog 3.22 and Nanolog spectrofluorimeters. Fluorescence microscopy have been recorded on an Axioplan 2ie Zeiss imaging microscope equipped with a NikonDXM1200F digital camera and Leica DMIRB fluorescence microscope. Optical microscopy images have been acquired on a Leica ICC50 W. Dynamic light scattering measurements were carried out on a SZ-100 Nanoparticle Analyzer (HORIBA) instrument operating at 22 °C.

Small angle X-ray scattering

SAXS data have been performed on the NCD beamline at the synchrotron ALBA at 12.4 keV and the distance sample/detector was 2.2m to cover the range of momentum transfer 0.09 < q <5.6 nm^{-1}. The data were collected on an ImXPad S1400 detector with a pixel size of 130.0x130.0μm^2. The exposure time was 10s. The q-axis calibration was obtained by measuring silver behenate.[26] The program pyFAI[27] was used to integrate the 2D SAXS data into 1D data.

The data were then subtracted by the background using *PRIMUS* software.[28] The maximum particle dimension D_{max} and the pair-distance distribution function $P(r)$ were determined with *GNOM*.[29] The low-resolution structure of the aggregates was reconstructed ab initio from the initial portions of the scattering patterns using the program DAMMIN.[30]

$1 \cdot 10^{-4}$ M and $1 \cdot 10^{-5}$M solutions of complexes **1a-b** and **2a-b** were prepared in different water/DMSO mixtures, between 0% water to 100% (0, 25, 50, 75, 90%).

Synthesis of [Au(C≡C-$C_{15}H_{10}N_3$)(PTA)] (1a). Solid PTA (21 mg, 0.13 mmol) was added to a suspension of $[Au(C{\equiv}C\text{-}C_{15}H_{10}N_3)]_n$ (60 mg, 0.13 mmol) in CH_2Cl_2 (20 mL). After 45 min of stirring at room temperature, the resulting pale yellow solution was concentrated (5 mL), and *n*-hexane (15 mL) was added to precipitate a pale yellow solid (66 mg, 81 %). ^{31}P-NMR (161.9 MHz, $CDCl_3$, ppm): -12.8. ^{1}H-NMR (400 MHz, $CDCl_3$, 298 K, ppm): 8.62 (*dq*, *J* = 4.8 Hz, *J* = 0.8 Hz, 2H, H_9), 8.53 (*dt*, *J* = 12.0 Hz, *J* = 1.2 Hz, 2H, H_{12}), 8.46 (*s*, 2H, H_3 + H_5), 7.84 (*td*, *J* = 11.9 Hz, *J* = 1.4 Hz, 2H, H_{11}), 7.30 (*ddd*, 2H, *J* = 12.0 Hz, *J* = 4.8 Hz, H_{10}), 4.60 – 4.48 (AB *q*, *J* = 13.0 Hz, 6H, N-CH_2-N), 4.30 (*s*, 6H, N-CH_2-P). IR (KBr, cm^{-1}): 3425 (C-H), 2114 (C≡C), 1636 (C=N). ESI-MS (+) *m/z*: 611.137 ($[M + H^+]^+$, calc.: 611.139), 1243.250 ($[2M + Na^+]^+$, calc.: 1243.252).

Synthesis of [Au(C≡C-$C_{15}H_{10}N_3$)(DAPTA)] (1b). Solid DAPTA (30 mg, 0.13 mmol) was added to a suspension of $[Au(C{\equiv}C\text{-}C_{15}H_{10}N_3)]_n$ (60 mg, 0.13 mmol) in CH_2Cl_2 (20 mL). After 45 min of stirring at room temperature, the resulting pale yellow solution was

concentrated (10 mL), and *n*-hexane (10 mL) was added to precipitate a pale yellow solid (75 mg, 85 %). ^{31}P-NMR (161.9 MHz, $CDCl_3$, ppm): -10.2. ^{1}H-NMR (400 MHz, $CDCl_3$, ppm): 8.68 (*dq*, *J* = 5.0 Hz, *J* = 0.8 Hz, 2H, H_9), 8.56 (*dt*, *J* = 12.0 Hz, *J* = 0.8 Hz, 2H, H_{12}), 8.48 (*s*, 2H, H_3 + H_5), 7.82 (*td*, *J* = 11.8 Hz, *J* = 1.6 Hz, 2H, H_{11}), 7.30 (*ddd*, 2H, *J* = 12.0 Hz, *J* = 4.8 Hz, H_{10}), 5.78 (*d*, *J* = 20.0 Hz, 1H, H_{19a} N-C*H*$_2$-N), 5.66 (*dd*, *J* = 20.0 Hz, *J* = 12.0 Hz, 1H, H_{23a} N-C*H*$_2$-P), 4.94 (*d*, *J* = 16.0 Hz, 1H, H_{21a} N-C*H*$_2$-N), 4.70-4.64 (*m*, 2H, H_{17a} N-C*H*$_2$-P + H_{21b} N-C*H*$_2$-N), 4.15 (*dt*, *J* = 20.0 Hz, *J* = 4.0 Hz, 1H, H_{17b} N-C*H*$_2$-P), 4.06 (*d*, *J* = 20.0 Hz, 1H, H_{19b} N-C*H*$_2$-N), 3.87 (*s*, 2H, H_{24} N-C*H*$_2$-P), 3.57 (*dt*, *J* = 20.0/4.0 Hz, 1H, H_{23b} N-C*H*$_2$-P), 2.17 (*s*, 6H, CO-C*H*$_3$). IR (KBr, cm^{-1}): 3441 (C-H), 2116 (C≡C), 1640 (C=N). ESI-MS (+) *m/z*: 683.158 ([M+H]$^+$, calc.: 683.160); 705.139 ([M+Na]$^+$, calc.: 705.142.

Synthesis of [Au(C≡C-C$_{10}$H$_7$N$_2$)(PTA)] (2a). Solid PTA (25 mg, 0.16 mmol) was added to a suspension of [Au(C≡C-C$_{10}$H$_7$N$_2$)]$_n$ (60 mg, 0.16 mmol) in CH_2Cl_2 (20 mL). After 45 min of stirring at room temperature, the resulting yellow solution was concentrated (10 mL), and *n*-hexane (10 mL) was added to precipitate a pale yellow solid (77 mg, 90 %). ^{31}P-NMR (161.9 MHz, $CDCl_3$, ppm): -48.2. ^{1}H-NMR (400 MHz, $CDCl_3$, ppm): 8.73 (*d*, *J* = 5.0 Hz, 1H, H_9), 8.65 (*dd*, *J* = 12.0 Hz, *J* = 0.8 Hz, 1H, H_6), 8.36 (*dt*, *J* = 12.0 Hz, *J* = 4.8 Hz, 1H, H_{12}), 8.29 (*dd*, *J* = 8.4 Hz, *J* = 2.5 Hz, 1H, H_3), 7.80 (*m*, *J* = 8.0 Hz, *J* = 1.6 Hz, 2H, H_4+ H_{11}), 7.27 (*ddd*, *J* = 8.0 Hz, *J* = 4.0 Hz, *J* = 2.0 Hz, 1H, H_{10}), 4.60 – 4.48 (AB *q*, *J* = 13.0 Hz, 6H, H_{19b} N-C*H*$_2$-N), 4.30 (*s*, 6H, N-C*H*$_2$-P). IR (KBr, cm^{-1}): 3425 (C-H), 2104 (C≡C), 1640 (C=N). ESI-MS (+) *m/z*: 534.111 ([M + H$^+$]$^+$, calc.: 534.112), 556.092 ([M + Na$^+$]$^+$, calc.: 556.094).

Synthesis of [Au(C≡C-C$_{10}$H$_7$N$_2$)(DAPTA)] (2b). Solid DAPTA (36 mg, 0.16 mmol) was added to a suspension of [Au(C≡C-C$_{10}$H$_7$N$_2$)]$_n$ (60 mg, 0.16 mmol) in CH_2Cl_2 (20 mL). After 45 min of stirring at room temperature, the resulting yellow solution was concentrated (10 mL), and *n*-hexane (10 mL) was added to precipitate a pale yellow solid (82 mg, 85 %). ^{31}P-NMR (161.9 MHz, $CDCl_3$, ppm): -23.0. ^{1}H-NMR (400 MHz, $CDCl_3$, ppm): 8.75 (*dd*, *J* = 4.0 Hz, *J* = 0.6 Hz, 1H, H_9), 8.66 (*dd*, *J* = 8.0 Hz, *J* = 0.8 Hz, 1H, H_6), 8.37 (*dt*, *J* = 12.0 Hz, *J* =

0.8 Hz, 1H, $H_{12'}$), 8.32 (*dd*, *J* = 11.8 Hz, *J* = 0.4 Hz, 1H, H_3), 7.82 (m, 2H, $H_4 + H_{11}$), 7.28 (*ddd*, *J* = 12.0 Hz, *J* = 7.2 Hz, *J* = 0.6 Hz, 1H, H_{10}), 5.78 (*d*, *J* = 20.0 Hz, 1H, H_{19a} N-C*H*$_2$-N), 5.66 (*dd*, *J* = 20.0, *J* = 12.0 Hz, 1H, H_{23a} N-C*H*$_2$-P), 4.94 (*d*, *J* = 16.0 Hz, 1H, H_{21a} N-C*H*$_2$-N), 4.70 – 4.64 (*m*, 2H, H_{17a} N-C*H*$_2$-P + H_{21b} N-C*H*$_2$-N), 4.15 (*dt*, *J* = 20.0 Hz, *J* = 4.0 Hz, 1H, H_{17b} N-C*H*$_2$-P), 4.06 (*d*, *J* = 20.0 Hz, 1H, H_{19b} N-C*H*$_2$-N), 3.87 (*s*, 2H, H_{24} N-C*H*$_2$-P), 3.57 (*dt*, *J* = 20.0, *J* = 4.0 Hz, 1H, H_{23b} N-C*H*$_2$-P), 2.17 (*s*, 6H, CO-C*H*$_3$). IR (KBr, cm^{-1}): 3425 (C-H), 2104 (C≡C), 1640 (C=N). ESI-MS (+) *m/z*: 606.132 ($[M + H]^+$, calc.: 606.133), 1233.233 ($[2M + Na]^+$, calc.: 1233.241).

Computational Details

All quantum level calculations were performed with the Amsterdam Density Functional (ADF)[31] using dispersion-corrected density functional, ZORA-BLYP-D3(BJ).[32] Previous benchmark study on non-covalent interactions showed that it is essential to incorporate the dispersion correction.[33] Geometry optimizations of monomers and dimers were obtained with the TZ2P basis set. Geometry optimizations of tetramers were obtained with the TZP basis set and the bond energies have been computed with the TZ2P basis set (single point with the optimized structures). The small frozen-core approximation has been applied. Symmetry was applied and is denoted in the Table 1 and in the SI. Solvent effects in water and DMSO have been estimated using the conductor-like screening model (COSMO),[34] as implemented in the ADF program.[35,36] According to the work by Riley et al.[37] the dispersion correction does not need to be modified for solvated systems. The bond energy ΔE_{bond} of the dimers and tetramers is defined by equations 1 and 2 respectively:

$$\Delta E_{bond} = E_{dimer} - 2 \cdot E_{monomer} \quad (1)$$

$$\Delta E_{bond} = E_{tetramer} - 4 \cdot E_{monomer} \quad (2)$$

where $E_{tetramer}$ is the energy of the optimized tetramer, E_{dimer} is the energy of the optimized dimer and $E_{monomer}$ the energy of one of the 4 different optimized monomers used.

Results and Discussion

Synthesis and characterization

Complexes **1-2** were obtained by the same methodology previously described in the literature for [Au(C≡C-C_5H_4N)(PTA)][8] and [Au(C≡C-C_5H_4N)(DAPTA)].[9] A dichloromethane suspension of the previously synthesized [Au(C≡C-$C_{15}H_{10}N_3$)]$_n$ (for **1a** and **1b**) or [Au(C≡C-$C_{10}H_7N_2$)]$_n$ (for **2a** and **2b**) polymer was stirred with the PTA or DAPTA phosphine in a 1 : 1 ratio (Schemes 1 and 2). The reaction was maintained under stirring at room temperature for 45 min. Coordination of these phosphines (PTA, DAPTA) immediately gave yellow solutions that after concentration and addition of *n*-hexane, yielded the corresponding complexes quantitatively.

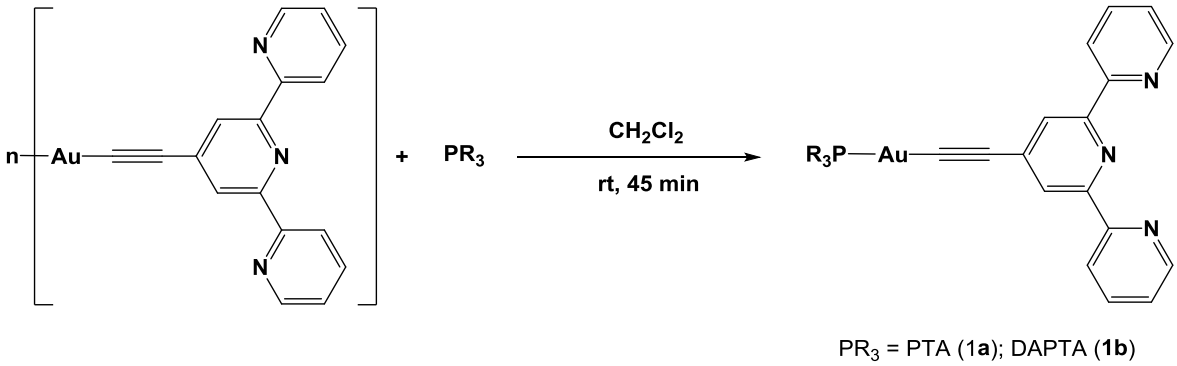

Scheme 1. Synthesis of [Au(C≡C-$C_{15}H_{10}N_3$)(PR_3)] (PR_3 = PTA (**1a**), DAPTA (**1b**)) complexes.

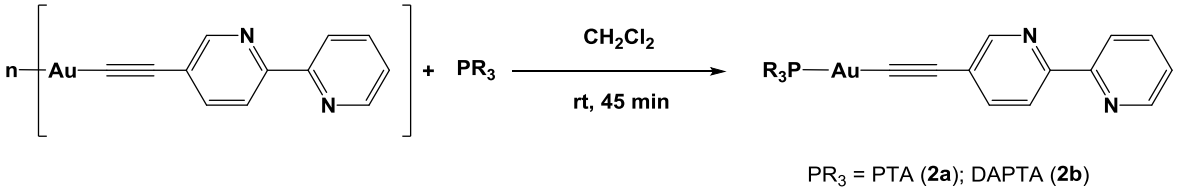

Scheme 2. Synthesis of [Au(C≡C-$C_{10}H_7N_2$)(PR_3)] (PR_3 = PTA (**2a**), DAPTA (**2b**)) complexes.

Characterization of complexes **1-2** by ^{1}H-, ^{31}P NMR, IR spectroscopy and mass spectrometry verified the successful formation of these products. Mass spectrometry measurements are able to detect the corresponding molecular peaks of the protonated species in all cases (see

SI). ^{1}H NMR spectra of the complexes recorded in $CDCl_3$ show the characteristic protons of the terpyridine[38-41] (**1a** and **1b**) and of the bipyridine[20,42] (**2a** and **2b**) together with the characteristic patterns of the PTA (**1-2a**) or DAPTA (**1-2b**) phosphines[8-11] (see SI). $^{31}P\{^{1}H\}$-NMR spectra carried out in $CDCl_3$ typically show one signal between -10 and -50 ppm, with a 50 (for PTA derivatives) or 30 (for DAPTA derivatives) ppm downfield shift in comparison with the free phosphines. The corresponding C≡C and C=N vibrations of the chromophoric units were also observed in the IR spectra in all the cases.

Aggregation in water and water/DMSO mixtures

As previously found for neutral gold(I) alkynyl complexes,[8-10] aged solutions of **1a-b** and **2a-b** in water give origin to the formation of luminescent fibers (see Figure S9) apparently originated from the merge of smaller aggregates[10] (see below SAXS and DLS discussion). The fibers are not observed from DMSO and chloroform solutions in the same time scale.

In D_2O, terpyridyl and bipyridyl protons are not observed in ^{1}H-NMR, even under highly diluted conditions (Figure 1), while the phosphine protons are clearly seen, even if slightly broader than in $CDCl_3$. The absence of the terpyridyl and bipyridyl proton signals is an expected result from aggregation, due to the slower mobility of the aggregates. What is unexpected is that the phosphine protons are still detected in the aggregates, since the restriction in mobility should apply to both parts of the molecule.

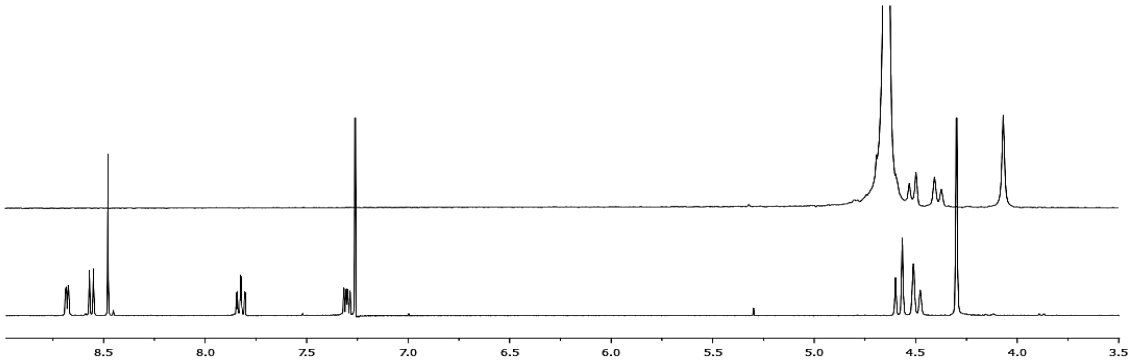

Figure 1. ^{1}H-NMR spectra (400 MHz) of compound **1a** in D_2O (top) and $CDCl_3$ (bottom) at $5\cdot10^{-4}$M concentration and 298 K.

In order to obtain a deeper knowledge on the self-assembling process at the molecular level, we performed a series of NMR spectroscopy studies in D_2O/DMSO-d_6 mixtures, due to the good miscibility of both solvents and to the complete solubilization of the molecules in DMSO-d_6 (Figure S10) having a comparable behavior to the previously observed in $CDCl_3$. We must point out that the very large aggregates are invisible in conventional solution NMR experiments due to the large line-broadening produced by the very efficient transverse relaxation in large molecular entities. The ^{1}H-NMR spectrum of **2b** in pure DMSO-d_6 showed well-resolved signals implying the major presence of discrete species (Figure 2c, black trace and S9) suitable assigned by 2D ^{1}H-^{13}C HSQC and HMBC experiments (Figures S11-12). However, two sets of signals were clearly observed in a 63:37 proportion suggesting the presence of two species in solution (with notation H and H' in Figure 2). The NOESY spectrum of this sample showed a cross-peak between the H_6' signal and the methyl signal of the acetyl of the DAPTA moiety, suggesting that the minor species should locate the bipyridyl and the DAPTA moieties in a relatively close proximity (Figure S13).

The DOSY experiment (Figures S14-15) rendered an apparent molecular size corresponding to a dimer structure for the two observed species (Table S2, hydrodynamic radius of 7.3 and 8.6 Å for the minor and major species, respectively). Accordingly, we assigned the minor species to the chain dimer and the major one to the stacked dimer (Figure 3). Very interestingly, the measured longitudinal and transverse relaxation times (Table S1) are unexpectedly long for discrete organic molecules in solution. Moreover, the magnetic relaxation of the signals from the bipyridyl moiety showed to be less efficient than the relaxation of the DAPTA moiety. This can be due to some rigidity of the bipyridyl group, although no definitive conclusions can be drawn due to the implication of the DAPTA moiety in a *cis/trans* dynamic process of the corresponding tertiary amide groups. Actually, the molecular system is implicated in different exchange processes that occurred at very different timescales (as observed by EXSY peaks in the NOESY experiments (Figure S13)).

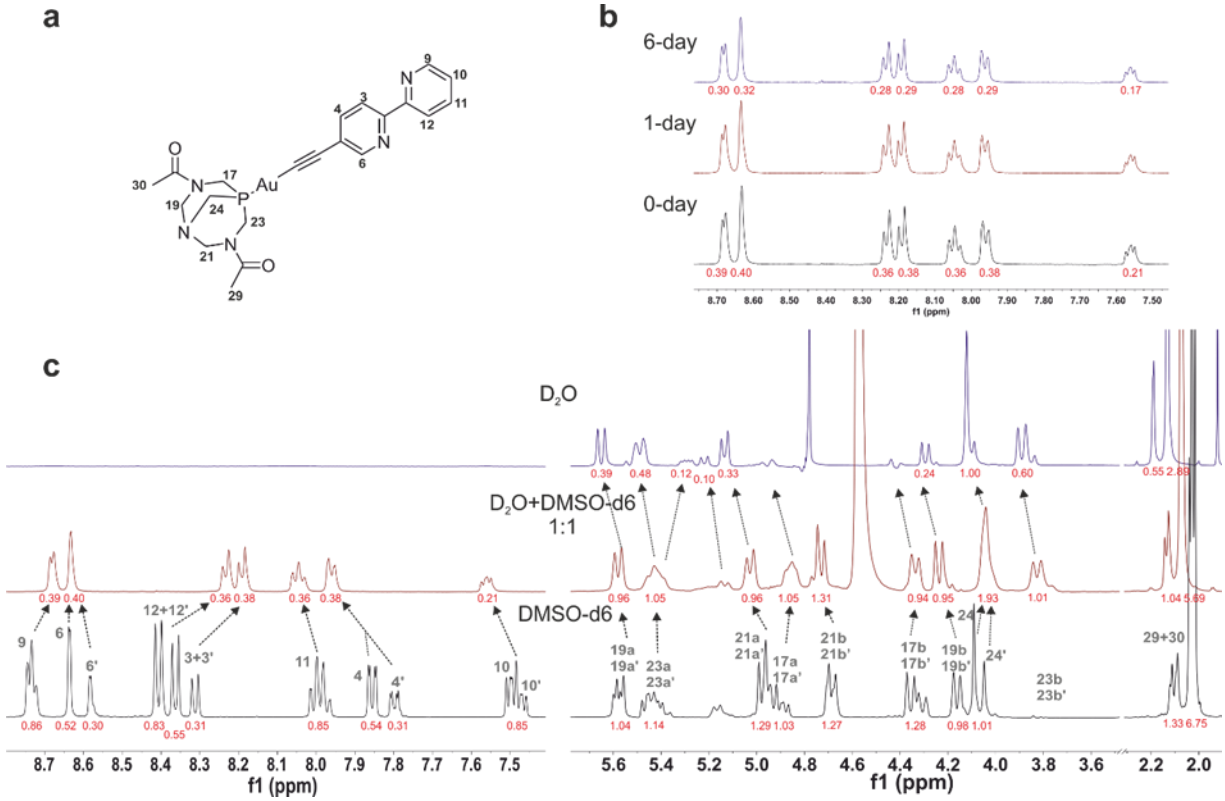

Figure 2. a) Chemical structure of **2b** with labelling numbers used in the NMR assignment; b) ^{1}H-NMR spectra (aromatic region) of 1 mM **2b** at different times after dissolution in D_2O:DMSO-d_6 (1:1); c) ^{1}H-NMR spectra of 1mM **2b** in different solvent conditions. The experiments were acquired at 500 MHz and 298K, with a relaxation delay of 20 s. Below the peaks, the numbers in red are the normalized peak area values (integral).

Thus, the amide *cis/trans* isomerization of DAPTA is slow in the chemical shift NMR timescale and can be observed by exchange cross-peaks in the NOESY experiments at 250 ms. Additionally, the exchange between the two dimeric species (chain/stacked, Figure 3) is slow in both the NMR chemical shift and NOESY timescales (exchange slower than 0.5 s). The complexity of the systems is even higher when looking at the integrals of the ^{1}H NMR signals. The ^{1}H NMR spectrum acquired at quantitative conditions (with a relaxation delay of 20 s) showed that the intensity of the bipyridine signals is lower than the ones for the DAPTA, once again suggesting that the bipyridyl ring is closely implicated in the self-assembling process. Besides, the comparison of the integrals of the observed NMR signals with that of an internal standard showed that about 10% of the molecule remains undetected

in solution NMR, suggesting the presence of large aggregates even in pure DMSO-d_6. The apparent lower motion of the bipyridyl rings is also observed in the negative NOE cross-peaks that imply a longer apparent tumbling time of this part of the molecule.

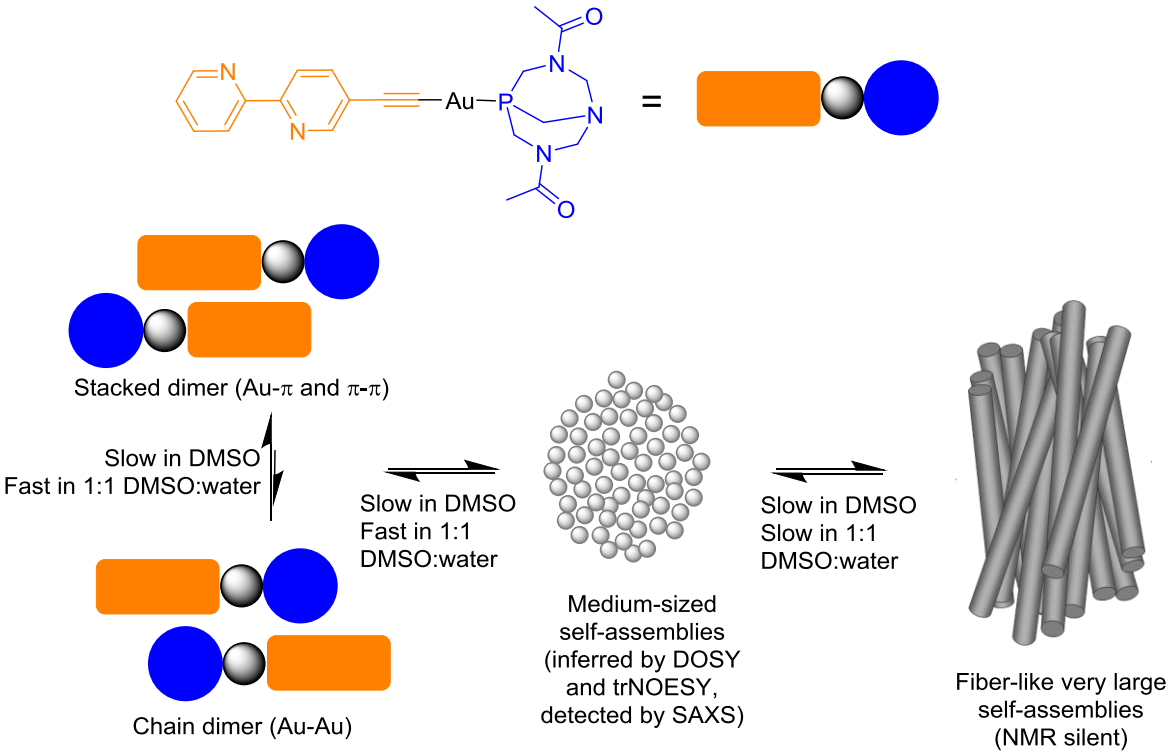

Figure 3. Schematic representation of the possible aggregates observed in solution.

To study the effect of water on the self-assembling, we performed a titration of the sample initially prepared in DMSO-d_6 with increasing amounts of D_2O (Figure S16). The increase of the polarity of the medium produced changes in the bipyridyl protons signals that are in agreement with the previously reported behavior.[43] All the signals broadened and the protons corresponding to the two dimeric species started to approach their chemical shifts (without an apparent variation in the proportion of species). This suggests that the presence of water accelerates the exchange between the two dimeric species. The DOSY experiment at 20% water in DMSO showed the clear presence of the two dimeric species with an apparent size similar to the one observed in pure DMSO (Table S2, Figure S17). However, the ^{1}H NMR signals coalesce at 1:1 DMSO-d_6:D_2O mixture, in which a single set of signals was observed for the bipyridyl moiety (Figure 2c, red trace). The NOESY spectrum of this sample showed peaks that are compatible with the two dimeric structures, implying that a fast exchange must

occur between the chain and the stacked species in this solvent mixture (Figure S18). This is also supported by the negative sign of the NOESY peaks, implying an apparent larger size of the species in solution rendering transferred NOESY effects between the dimeric species and larger aggregates. The integrals of the protons in the 1D ^{1}H spectrum suggested a higher proportion of the invisible aggregates, while the DOSY experiments (Figure S19) rendered values compatible with the presence of dimeric species and in equilibrium with larger aggregates (hydrodynamic radius of 7.8 and 15.0 Å for different signals of the spectrum, Table S2). Moreover, acquisition of the ^{1}H NMR spectrum after longer preparation times showed a decrease of the intensity signals with time (Figure 2b), implying a slow formation of very large self-assemblies (6 days).

Finally, the ^{1}H NMR spectrum of a sample prepared in pure water showed a further decrease of the intensity of the protons of the DAPTA and the complete disappearance of the signals from the bipyridyl moiety (Figure 2c, blue trace). The NOESY spectrum of this sample (Figure S20) showed spin diffusion effects in agreement with the formation of very large aggregates in solution where the bipyridine would be less accessible to the solvent, leading to a large broadening up to undetectable signals. A faster dynamic and solvent exposure of the DAPTA fragments allowed the detection of their NMR signals. The same behavior was observed for the complex [Au(C≡C-$C_{10}H_7N_2$)(PTA)] (**2a**) in pure DMSO-d_6 and 1:1 DMSO-d_6 : D_2O mixture (Figures S21-S26).

^{31}P-NMR experiments recorded in different DMSO- d_6 : D_2O proportions are in agreement with these data. A broad signal is observed in pure DMSO-d_6 implying the existence of different conformations in slow equilibrium. Moreover, the increase of amounts of D_2O shifts to a sharp and clearly defined downfield peak as expected when the equilibrium between chain and stacked conformation becomes faster in D_2O. (Figures S27-28).

Considering all these NMR results, a putative self-assembling mechanism for **2a** and **2b** gold(I) complexes is proposed in Figure 3.

The aggregation has visible impact on the optical properties of the solutions, both in the absorbed and emitted light. With the increase in water content, there is a clear change of the absorption towards the visible region, displayed by the yellowing of the solutions, and at the same time, the strong blue emission observed in DMSO is quenched at increasing amounts of water and replaced by a red emission (Figure 4 and S29).

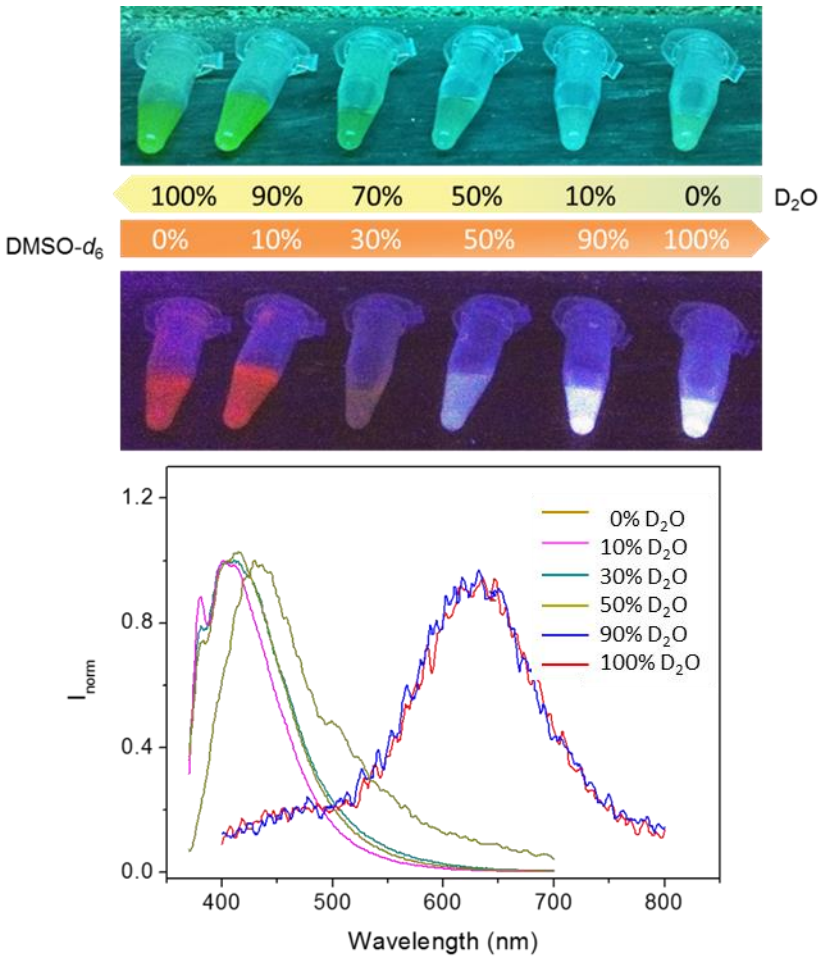

Figure 4. Variation of color of $1 \cdot 10^{-4}$M D_2O/DMSO-d_6 solutions of **2b** under visible and UV light (above); Normalized emission of **2b** at different compositions of DMSO-d_6:D_2O (λ_{exc} = 360 nm).

The lower energy band at ca. 630 nm is assigned to the aggregates, where the presence of excimers due to π–π stacking or Au-π stacking can both contribute to the broad shape and red-shift of the band.[11] These interactions seem to be more favored in water, in agreement with theoretical calculations (see below). The higher emission band at 430 nm is assigned to ^{1}MLCT/^{1}LLCT transition, being more favored in DMSO, due to the presence of chain conformation, which allows the free movement of the phosphane and polypyridine moieties of the compounds in the aggregates (mainly aurophilic interactions).

Small Angle X-ray scattering measurements (SAXS) were performed for $1 \cdot 10^{-5}$ M and $1 \cdot 10^{-4}$ M solutions of the compounds in different water/DMSO proportions. The low-resolution structures were reconstructed *ab initio* from the scattering patterns with the use of the program DAMMIN[30] and are shown in Figure 5 and S30-32 for two concentrations and two solvent compositions.

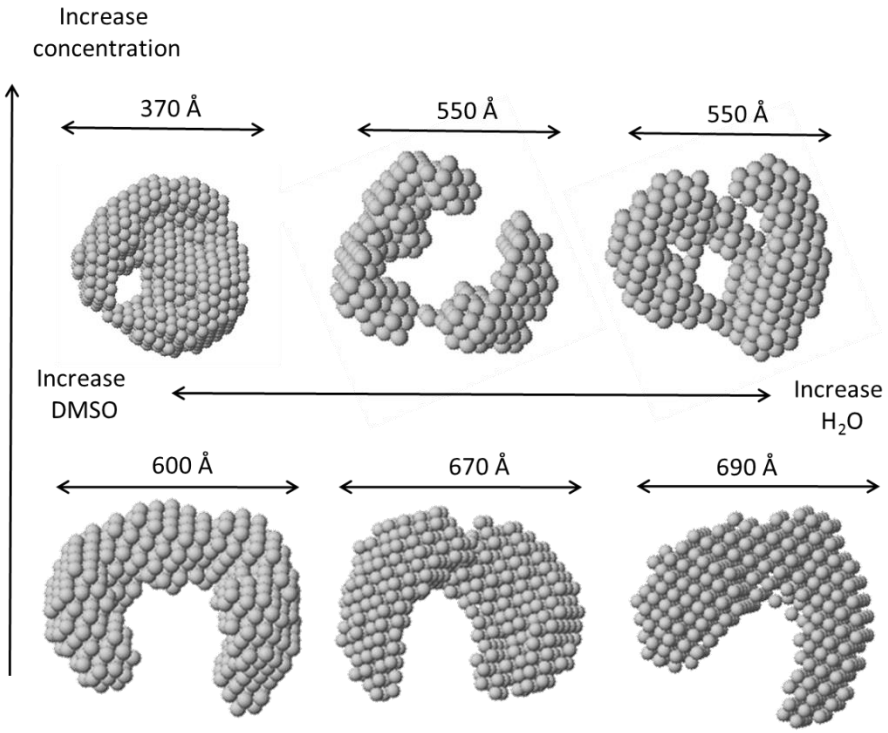

Figure 5. DAMMIN low resolution structures reconstructed from SAXS scattering patterns for $1x10^{-4}$ M (top) and $1x10^{-5}$ M (bottom) solutions of **2a** in DMSO (left), water:DMSO 1:1 (centre) and H_2O : DMSO 3:1 (right).

The observation is that in all mixtures, the large aggregates show comparable dimensions at the same concentration, independently of solvent composition and, in general, a slight increase in the size of aggregates is shown with the increase in water concentration. There is no significant difference in size between terpyridyl and bipyridyl derivatives (Figure 5 and S30-32). This result suggests that aggregates exist in the different water/DMSO mixtures of solvents and the differences observed may arise from internal reordering of the aggregates (chain/stacked aggregates detected by NMR and luminescence). Additionally, temperature does not affect significantly the size nor the shape of the resulting structures (Figures S33-36).

Dynamic Light Scattering measurements were in agreement with the presence of aggregates in DMSO at $1 \cdot 10^{-4}$ M concentration. The presence of ca. 100 nm size supramolecular structures is observed in all cases (see Figures S37-40). As expexted, the size of the aggregates obtained by DLS and SAXS are much larger than the hydrodynamic radius previously calculated by NMR DOSY experiments (see above). SAXS/DLS and NMR techniques are complementary regarding the detected assembly size: due to the slow tumbling of larger macromolecules in solution leading to faster relaxation of transverse magnetization, only the soluble dimers and small aggregates in equilibria with the larger assemblies (detecteb by SAXS/DLS) are observed by NMR (the larger structures are "invisible" in solution NMR) .

Computational Study of the aggregation modes

We have computationally analyzed the structures of **1a-b** and **2a-b** (see Figure S41) and their auto-association properties to form different dimers and tetramers (as a model for larger aggregates).

We have analyzed different dimerization and tetramerization possibilities for each one of the monomers in Figure S41, involving different arrangements of ligand-ligand interactions, gold-gold interactions and ligand-gold interactions (see Figure 6 and 7).

An important difference between the tetramers calculated is that in stacked conformation the main contribution arises from gold-π interactions, in double dimer there are contributions from gold-gold and π - π interactions, while in chain conformation the main contribution is a continuous chain of gold-gold interactions that grows with aggregate size. The gold-gold distances between successive monomeric units in the tetramers and the bond energies are summarized in Table 1.

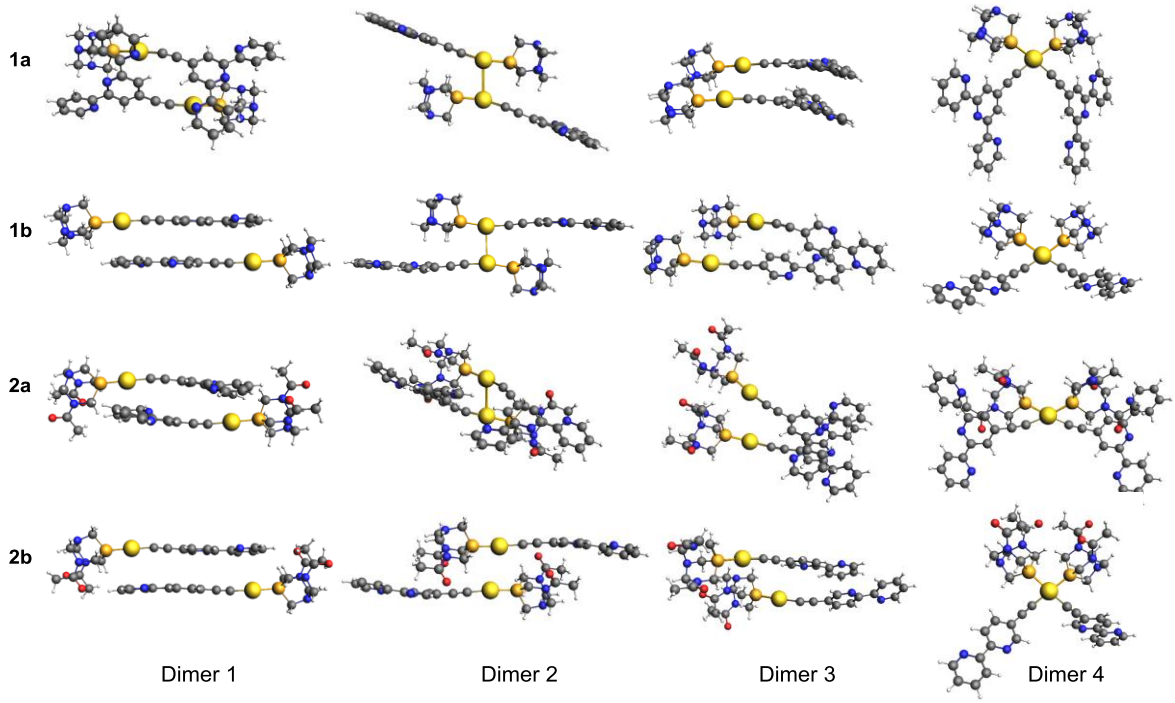

Figure 6. Structures of the computed dimers.

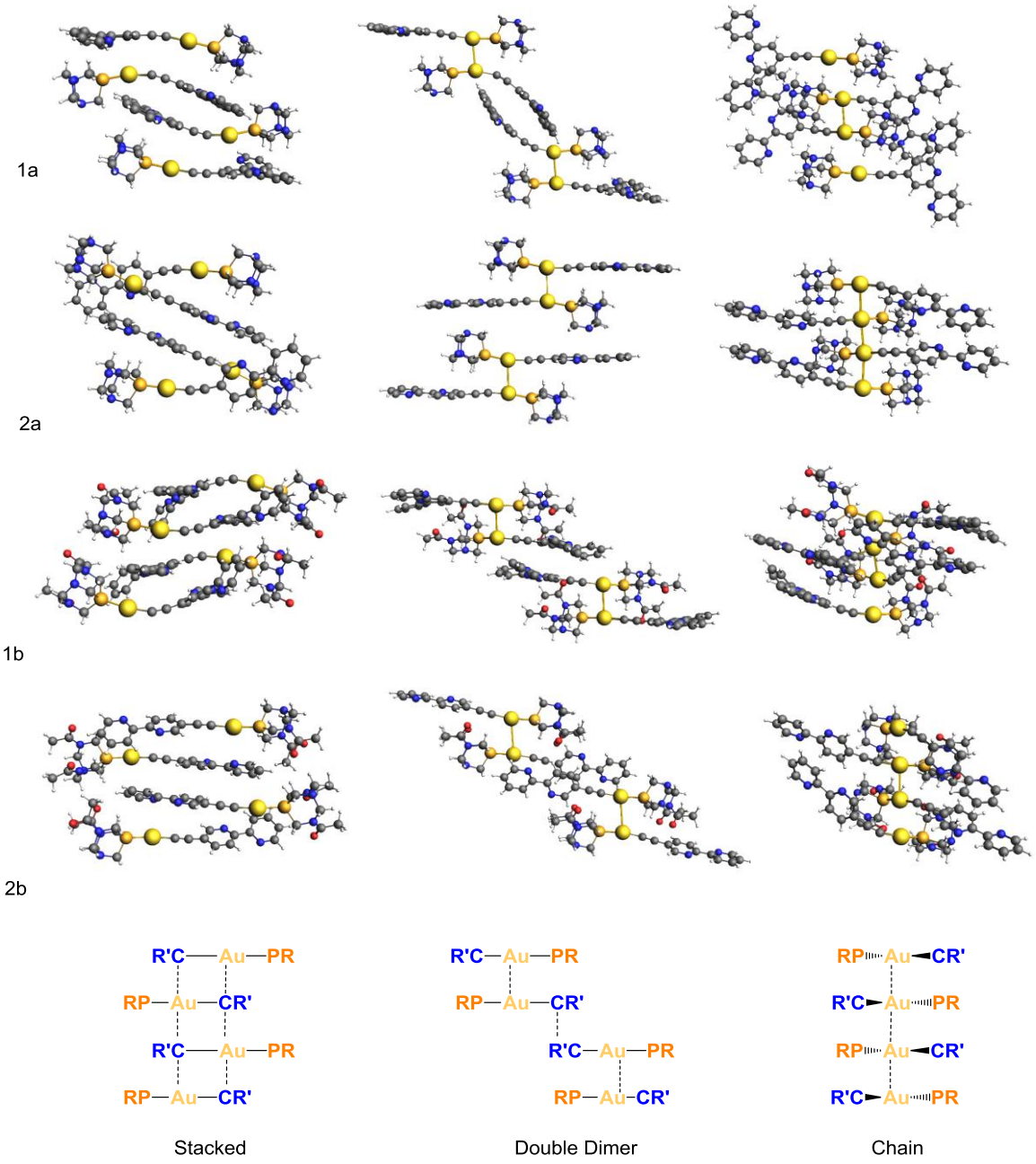

Figure 7. Structures of the computed tetramers and schematic representation.

Table 1 Au–Au distances[a] (in Å) and bond energies[b] (in kcal/mol) of the tetramers of **1a-b** and **2a-b** in water.

1a	Stacked, C_{2h}	Double Dimer, C_{2h}	Chain, C_2
Au1–Au2	5.99	3.27	4.13
Au2–Au3	10.44	11.59	3.16
Au3–Au4	5.99	3.27	4.13
ΔE_{bond}	-56.8	-41.8	-65.0
2a	Stacked, C_{2h}	Double Dimer, C_1	Chain, C_1
Au1–Au2	5.96	3.29	3.07
Au2–Au3	11.10	6.97	3.00
Au3–Au4	5.96	3.28	3.10
ΔE_{bond}	-57.9	-42.0	-67.6
1b	Stacked, C_i	Double Dimer, C_2	Chain, C_1
Au1–Au2	9.73	3.26	3.18
Au2–Au3	6.77	11.48	3.13
Au3–Au4	9.73	3.26	3.16
ΔE_{bond}	-60.2	-42.5	-81.4
2b	Stacked, C_i	Double Dimer, C_i	Chain, C_1
Au1–Au2	9.64	3.59	3.22
Au2–Au3	12.35	11.46	3.07
Au3–Au4	9.64	3.59	3.23
ΔE_{bond}	-56.1	-36.0	-70.0

[a] Structure of tetramers computed at ZORA-BLYP-D3(BJ)/TZP level of theory with COSMO approximation for the solvent (water).

[b] Bond energies computed at ZORA-BLYP-D3(BJ)/TZ2P level of theory with COSMO approximation for the solvent (water).

Note that with no exception, there is a non negligible stabilization of the chain conformation in the tetramers. The same is not observed for the bond energy of the dimers, collected in Table 2. For the dimers, the conformations with shorter gold-gold distances (Dimer2 and Dimer4, gold···gold interactions) are not more stable than the conformations with favored ligand-ligand interactions, either in head to tails (dimer 1; π···gold interaction) or head to head (dimer 3; π-π interaction) conformations (see Figure 6). That is, the formation of the dimers in water in stacked conformation is more favored according to these calculations (in agreement with luminescence data), while the predicted stability of larger structures does not

seem to be so straightforward, since entropic factors (not considered here) should be more important in the presence of π···gold interactions.

Table 2. Au–Au distances (in Å) and bond energies[a] (in kcal/mol) of the tetramers of **1a-b** and **2a-b** in water.

1a	Dimer1	Dimer2	Dimer3	Dimer4
Au-Au distance	6.20	3.39	4.72	3.22
ΔE_{bond}	-21.1	-11.1	-20.2	-18.5
2a	Dimer1	Dimer2	Dimer3	Dimer4
Au-Au distance	11.67	3.24	5.33	3.34
ΔE_{bond}	-21.2	-14.5	-22.2	-15.5
1b	Dimer1	Dimer2	Dimer3	Dimer4
Au-Au distance	9.50	3.30[b]	4.41	3.17
ΔE_{bond}	-25.0	-14.7[b]	-18.7	-11.7
2b	Dimer1	Dimer2	Dimer3	Dimer4
Au-Au distance	11.42	3.86	5.41	3.25
ΔE_{bond}	-20.0	-8.6	-22.3	-13.0

[a] Bond energies of dimers computed at ZORA-BLYP-D3(BJ)/TZP level of theory with COSMO approximation for the solvent (water).
[b] Structure of dimer2 of **1b** is close to the structure of dimer4.

Another distinct aspect of the aggregation modes is related with the impact of the aggregates on the observables from either NMR, SAXS and optical spectroscopies. For all the tetramers the favored aggregation modes are either stacked or chain aggregation. On the contrary, while chain aggregation allows minimizing hydrophobic interactions of the chromophoric unit and maximizes exposure to the solvent, the stack aggregation maximizes the hydrophobic gold···π interaction, pulling the chromophoric unit to the core of the aggregate while allowing the phosphine unit full exposure to the solvent. The stack aggregation thus, is compatible with the excitonic interaction displayed both in the absorbed light (yellowing) and emitted light (quenching and red shift) and can be the major species observed when increasing the amount of D_2O in luminescence studies. By the same argument, the chain aggregation is more compatible with the optical spectroscopy data obtained in DMSO, where both aromatic and phosphine protons are exposed to the solvent and the chromophore absorption in the UV together with the blue emission is recovered. At the same time, a second species (chain conformers) is detected in ^{1}H-NMR spectra recorded in pure DMSO-d_6. Calculations performed in DMSO support this fact (Table S3). It can be seen that the

contribution of the chain conformation becomes more important in this solvent, mainly in the bipyridyl complexes. In fact, the charge transfer (CT) contribution observed in the case of the gold···gold interactions[44] increases with the number of gold atoms involved in the chain and while a single gold···gold bond is of the same order of magnitude as other interactions (gold···π and π···π stacking). With the growth of the number of gold atoms, these interactions become more important in the stabilization of the aggregates.

We can not forget that theoretical calculations take into consideration bonding energy, while some entropic aspects, like hydrophobic interactions (expected to be more important for terpyridyl complexes), have a direct impact on the aggregation.

Reversible Aggregation/dissaggregation processes

The presence of N-donor atoms in the chemical structure of the complexes makes these systems ideal candidates for cation coordination. The main important point in this work is that coordination of cations may have a direct influence on the resulting aggregates being able to externally modulate the formation/dissolution of the supramolecular structures. The initial solutions display the typical π-π* ($C{\equiv}C\text{-}C_{15}H_{10}N_3$) (for **1a**-**b**) or π-π*($C{\equiv}C\text{-}C_{10}H_7N_2$) (for **2a**-**b**) absorption transitions of chromophores between 310-360 nm.[20,45,46] Additionally, a band at higher energy (ca. 280 nm) due to the intraligand absorption of the phosphine is also recorded and another band at lower energy and with very low intensity between 360-400 nm is also present, which is assigned to a $\sigma^*_{(Au\text{-}Au)} \rightarrow \pi^*$ transition in agreement with previous data based on theoretical and thermodynamic calculations[44,47] (see Figure S42). In order to check the ability of the complexes to coordinate metal cations, aqueous solutions ($1x\ 10^{-4}$ M) of **1** and **2**(**a**-**b**) were titrated with Zn^{2+}, chosen as a divalent ion that can coordinate to N-atoms. Absorption and emission variations in the presence of increasing amounts of Zn^{2+} were detected and they are displayed in Figures 8 and S43-45.

An interesting feature is observed with increasing the amount of Zn^{2+}. The broad intraligand absorption band turns to some vibronic resolution profile with higher absorption. In the meanwhile, the red emission band disappears and a blue fluorescence, previously assigned to ^{1}MLCT, rises for DMSO solutions. Emission bands resulting from Zn^{2+}-coordination

present some vibronic resolution, typical of non-aggregated chromophores. Additionally, the resulting blue emission is much higher in intensity than the red aggregated emission, as observed in the water/DMSO solutions of the compounds.

The plot of the emission variations against Zn^{2+} concentration displays a change on slope at ca. 0.3 equivalents (Figure 8 right inset), which is an indication of a 1:3 (divalent cation : gold complex) coordination (Figure S46).

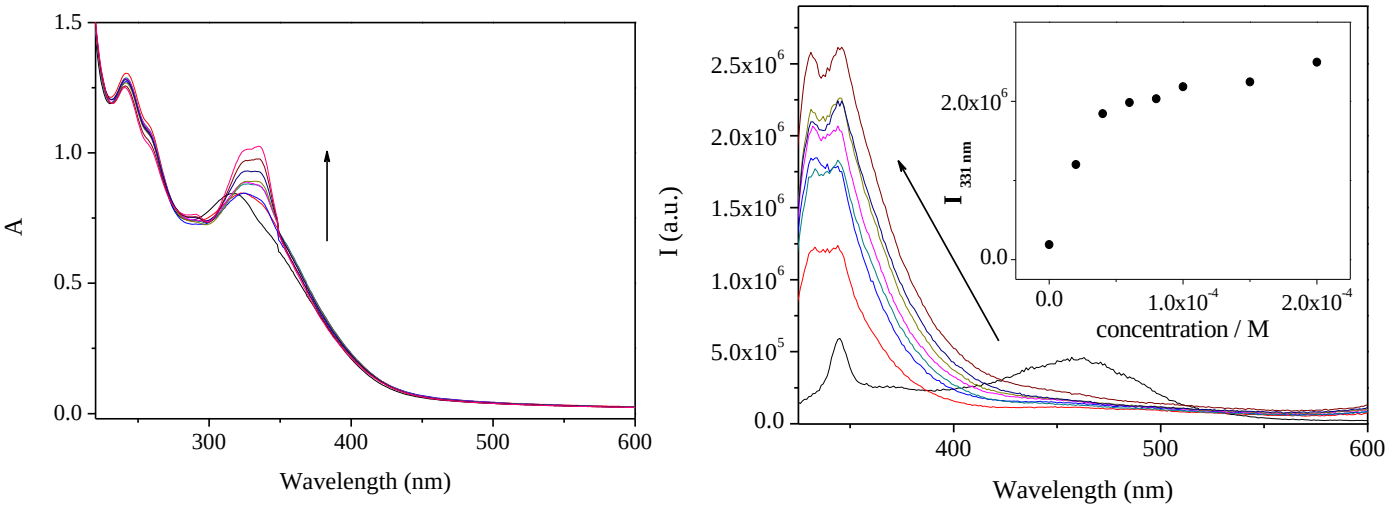

Figure 8. Absorption (left) and emission spectra of a $1 \cdot 10^{-4}$M aqueous solution of **2a** in the presence of increasing amounts of Zn^{2+}.

Interestingly, the red emission band appears again when a Zn^{2+} encapsulating agent (1,2-bis(3aminopropilamine)ethane, EDTA or 4,7,13,16,21,24-Hexaoxa-1,10-diazabicyclo[8.8.8]hexacosane cryptand) is added to the solution (see Figure S47), as a result of the Zn^{2+} entrapment. This means that the aggregation state can be directly modulated, being an effective example of adaptive supramolecular systems modulated by external stimuli.

As mentioned before, the intensity reduction of bipyridine resonances for pure **2b** in D_2O are related to the longer rotational correlation times (τ_C) and shorter T_2 associated to the assembly process. Therefore, this assembly/disassembly process could be followed by monotoring the

intensity changes on the NMR spectra. Addition of Zn^{2+} to a solution of **2b** in D_2O produced the intensity recovery of the proton NMR signals of the bipyridyl moiety. The observed chemical shifts of this fragment are in agreement with a coordination of the Zn^{2+} ion to the bipyridine ring in a *syn* disposition of the nitrogen atoms.[48] The complexation of Zn^{2+} cations with an excess of complexing agent cryptand partially reverted the disassembly effects of Zn^{2+}, as observed by the concomitant decrease of the intensity of the aromatic signals in the upper spectrum of Figure 9. The presence of an excess of Zn^{2+} also shifted the DAPTA proton signals suggesting a marginal interaction with the tertiary nitrogen or the amide carbonyls of DAPTA (Figure 9).

SAXS experiments performed in the presence of Zn^{2+} and the following addition of encapsulating agent show that the enclosed structure of the gold(I) complexes in water (Figure 10 left) is disturbed in the presence of the divalent cation (Figure 10 middle) giving rise to smaller structures and going back to aggregation when the encapsulating agent traps the cation and allows the gold(I) complex to self-assemble again (Figure 10 right, and Figures S48-50).

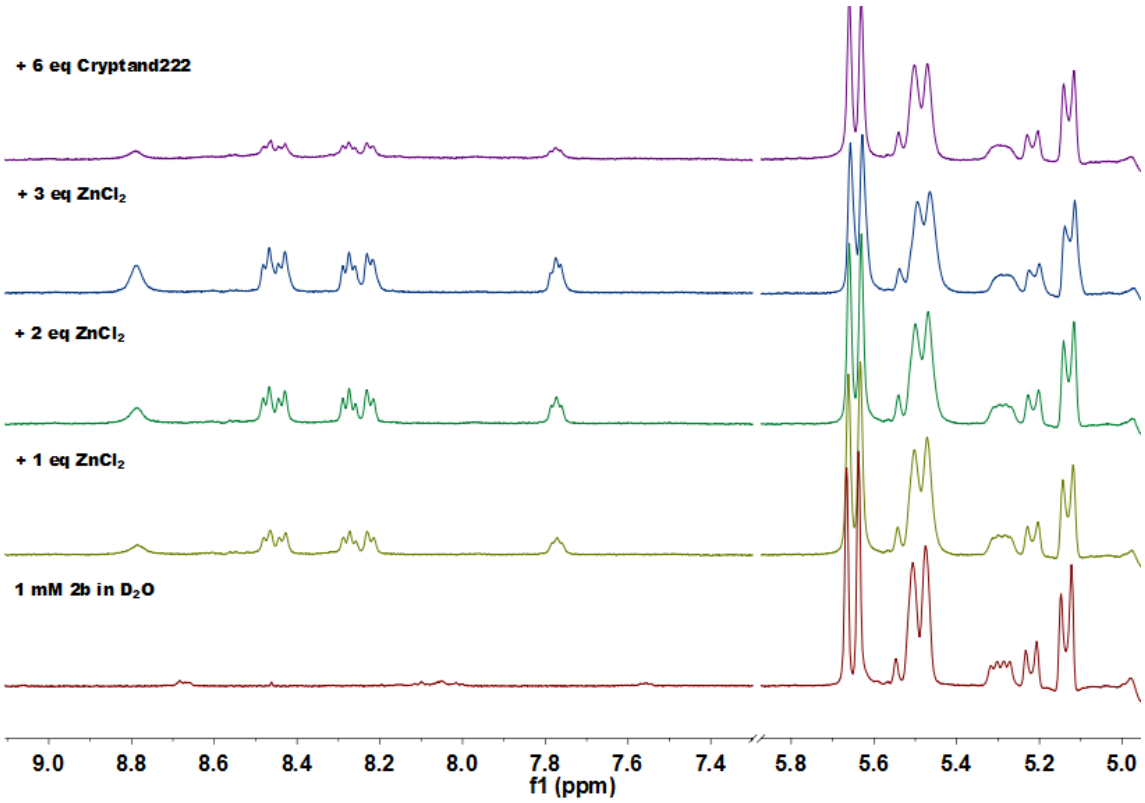

Figure 9. ^{1}H NMR spectra of 0.9 mM [Au(C≡C-$C_{10}H_7N_2$)(DAPTA)] in D_2O and with increasing amounts of metal (1, 2 or 3 equivalents of $ZnCl_2$) and after addition of 6 equivalents of cryptand to the sample with 3 equivalents of Zn^{2+}.

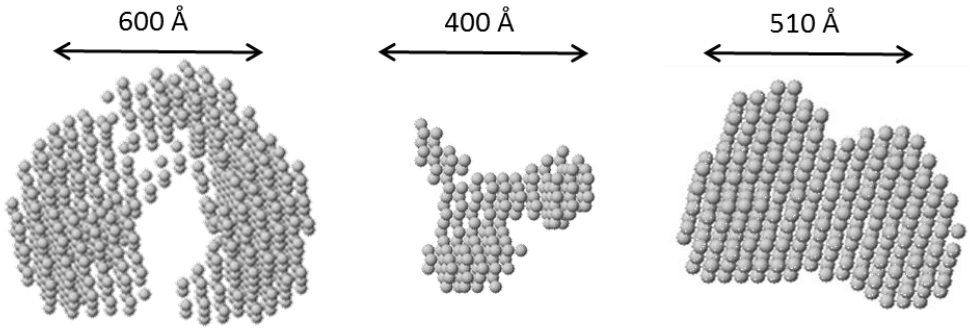

Figure 10. DAMMIN low resolution structures reconstructed from SAXS scattering patterns for 1x10^{-4} M of **2a** (left) in water; in the presence of 1 equivalent of Zn^{2+} (middle) and in the presence of 1 equivalent of Zn^{2+} and cryptand (right).

These processes were observed also for samples in solution under optical microscopy. Well-organized fibrilar aggregates can be detected for an aqueous solution of the complexes that disaggregate in the presence of Zn^{2+} and come back to aggregation when an encapsulating agent is added to the solution (Figure S51).

All in all, we have demonstrated for the first time the self-aggregation of discrete gold(I) complexes in water that can be externally modulated by the presence/absence of a divalent cation. This process is reversible and has been detected by complementary techniques: NMR, absorption, emission, SAXS, DLS and optical microscopy in solution.

Conclusions

Gold(I) alkynyl complexes containing bipyridine and terpyridyne π-systems, and water soluble phosphines (PTA and DAPTA) self-assemble in water and in DMSO, as shown by SAXS, NMR and DLS, with very distinct luminescence displayed in both solvents.

An exhaustive ^{1}H-NMR study performed with different D_2O/DMSO mixtures indicates the presence of two different assembly modes in the aggregates: chain assemblies that are based mainly on aurophilic interactions and stacked assemblies which are based on Au⋯π interactions, which are confirmed by DFT theoretical calculations carried out in both solvents. The initial aggregates of nanometers size merge with time to the formation of fibers. This process is promoted by the presence of water.

Bipyridine and terpyridine groups can complex metal cations, leading to the disassembly of the aggregates in the presence of Zn^{2+}. This process can be reverted by the addition of complexing agents that sequester Zn^{2+}.

The supramolecular assemblies respond to metal ion content by significant changes in both the morphology and luminescence. On a speculative note, the system can constitute the basis of a supramolecular adaptative system, towards the presence of metal cations and biological macromolecules able to compete for metal complexation in cells.

Acknowledgements

Authors are also grateful to the Ministry of Economy, Industry and Competiveness of Spain (AEI/FEDER, UE Project CTQ2016-76120-P, CTQ2015-65040-P and CTQ2015-70117-R). This work was also supported by the Associated Laboratory for Sustainable Chemistry-Clean Processes and Technologies-LAQV, which is financed by national funds from FCT/MEC (UID/QUI/50006/2013) and co-financed by the ERDF under the PT2020 Partnership Agreement (POCI-01-0145-FEDER-007265). IQAC NMR Facility 500 MHz Spectrometer and CryoProbe were funded by CSIC13-4E-2076 MINECO-FEDER grant. SAXS experiments were performed at the NCD-BL11 beamline of the Alba Synchrotron Light Facility with the collaboration with ALBA staff. A.M. thanks FCT for a post-doctoral grant (SFRH/BPD/69210/2010). This research was supported by a Marie Curie Intra European Fellowship within the 7th European Community Framework Programme (R.G.). We also would like to thank L. Giménez and I. Brea for the help on the synthesis of the ligands.

Supporting Information

1D and 2D NMR data, UV-visible and luminescent spectra, SAXS data, DLS data, Fluorescence and Optical microscopy images of the compounds at different conditions. Schemes of the synthesis of the complexes and precursors. Tables with NMR data and with theoretical calculations parameters. The Supporting Information is available free of charge on the ACS Publications website.

References

[1] Mayoral Muñoz, M. J.; Fernández, G. Metallosupramolecular amphiphilic π-systems. *Chem. Sci.*, **2012**, *3*, 1395.

[2] Sun, Q.-F.; Iwasa, J.; Ogawa, D.; Ishido, Y.; Sato, S.; Ozeki, T.; Sei, Y.; Yamaguchi, K.; Fujita, M. Self-assembled M24L48 polyhedra and their sharp structural switch upon subtle ligand variation. *Science*, **2010**, *328*, 1144.

[3] Chui, S.S.Y.; Ng, M.F.Y.; Che, C.-M. C.-M. Structure Determination of Homoleptic AuI, AgI, and CuI Aryl/Alkylethynyl Coordination Polymers by X-ray Powder Diffraction. *Chem. Eur. J.* **2005**, *11*, 1739.

[4] Chow, A.L.-F.; So, M.-H.; Lu, W.; Zhu, N.; Che, C.-M. Synthesis, Photophysical Properties, and Molecular Aggregation of Gold(I) Complexes Containing Carbon-Donor Ligands. *Chem. Asian J.* **2011**, *6*, 544.

[5] Lin, Q.; Yang, Q.-P.; Sun, B.; Fu, Y.-P.; Zhu, X.; Weiand, T.-B.; Zhang, Y.-M. Competitive coordination control of the AIE and micro states of supramolecular gel: an efficient approach for reversible dual-channel stimuli-response materials. *Soft Matter*, **2014**, *10*, 8427.

[6] Lima, J. C.; Rodríguez, L. Applications of gold(I) alkynyl systems: a growing field to explore. *Chem. Soc. Rev*., **2011**, *40*, 5442.

[7] Pinto, A.; Svahn, N.; Lima, J.C.; Rodríguez, L. Aggregation induced emission of gold(I) complexes in water or water mixtures. *Dalton Trans.* **2017**, *46*, 11125.

[8] Gavara, R.; Llorca, J.; Lima, J. C.; Rodríguez, L. A luminescent hydrogel based on a new Au(I) complex. *Chem. Commun*., **2013**, *49*, 72.

[9] Aguiló, E.; Gavara, R.; Lima, J. C.; Llorca, J.; Rodríguez, L. From Au(I) organometallic hydrogels to well-defined Au(0) nanoparticles. *J. Mat. Chem. C*, **2013**, *1*, 5538.

[10] Moro, A. J.; Rome, B.; Aguiló, E.; Arcau, J.; Puttreddy, R.; Rissanen, K.; Lima, J. C.; Rodríguez, L. A coumarin based gold(I)-alkynyl complex: a new class of supramolecular hydrogelators. *Org. Biomol. Chem.*, **2015**, *13*, 2026.

[11] Aguiló, E.; Gavara, R.; Baucells, C.; Guitart, M.; Lima, J.C.; Llorca, J.; Rodríguez, L. Tuning supramolecular aurophilic structures: the effect of counterion, positive charge and solvent. *Dalton Trans.*, **2016**, *45*, 7328.

[12] Chan, A. K.-W.; Lam, W. H.; Tanaka, Y.; Wong, K. M.-C.; Yam, V. W.-W. Multiaddressable molecular rectangles with reversible host–guest interactions: Modulation of pH-controlled guest release and capture. *PNAS*, **2015**, *112*, 690.

[13] Aida, T.; Meijer, E. W.; Stupp, S. I. Functional supramolecular polymers. *Science*, **2012**, *335*, 813.

[14] Hubbell, J. A.; Chilkoti, A. Chemistry. Nanomaterials for drug delivery. *Science*, **2012**, *337*, 303.

[15] Bhring, S.; Martín-Gomis, L.; Olsen, G.; Nielsen, K.A.; Kim, D.S.; Duedal, T.; Sastre-Santos, A.; Jeppesen, J.O.; Sessler, J.L. Design and Sensing Properties of a Self-Assembled Supramolecular Oligomer. *Chem. Eur. J*., **2016**, *22*, 1958.

[16] (a) Arcau, J.; Andermark, V.; Aguiló, E.; Gandioso, A.; Moro, A.; Cetina, M.; Lima, J.C.; Rissanen, K.; Ott, I.; Rodríguez, L. Luminescent alkynyl-gold(I) coumarin derivatives and their biological activity. *Dalton Trans*. **2014**, *43*, 4426; (b) Gavara, R.; Aguiló, E.; Schur, J.; Llorca, J.; Ott, I.; Rodríguez, L. Study of the effect of the chromophore and nuclearity on the aggregation and potential biological activity of gold(I) alkynyl complexes. *Inorg. Chim. Acta* **2016**, *446*, 189; (c) Meyer, A.; Gutiérrez, A.; Ott, I.; Rodríguez, L. Phosphine-bridged dinuclear gold(I) alkynyl complexes: Thioredoxin reductase inhibition and cytotoxicity. *Inorg. Chim. Acta* **2013**, *398*, 72.

[17] Grosshenny, V.; Ziessel, R. Synthesis and properties of novel ditopic polypyridine ligands bridged by one and two acetylenic bonds. *Tetrahedron Lett.* **1992**, *33*, 8075.

[18] Ferrer, M.; Giménez, L.; Gutiérrez, A.; Lima, J.C.; Rodríguez, L.; Martínez, M.; Martín, A.; Puttreddy, R.; Rissanen, K. Polypyridyl-functionalizated alkynyl gold(I) metallaligands supported by tri- and tetradentate phosphanes. *Dalton Trans.* **2017**, DOI: 10.1039/c7dt02732j.

[19] Constable, E. C.; Housecroft, C. E.; Kocik, M. K.; Zampese, J. A. Photoactive building blocks for coordination complexes: Gilding 2,2′:6′,2″-terpyridine. *Polyhedron*, **2011**, *30*, 2704.

[20] Vicente, J.; Gil-Rubio, J.; Barquero, N.; Jones, P.G.; Bautista, D. Synthesis of Luminescent Alkynyl Gold Metalaligands Containing 2,2′-Bipyridine-5-yl and 2,2′:6′,2″-Terpyridine-4-yl Donor Groups. *Organometallics*, **2008**, *27*, 646.

[21] Aguilar, J. A.; Nilsson, M.; Bodenhausen, G.; Morris, G. A. Spin echo NMR spectra without J modulation. *Chem. Commun.*, **2012**, *48*, 811.

[22] Johnson, C. S. Diffusion ordered nuclear magnetic resonance spectroscopy: principles and applications. *Prog. Nucl. Magn. Reson. Spectrosc.*, **1999**, *34*, 203.

[23] Nilsson, M. The DOSY Toolbox: a new tool for processing PFG NMR diffusion data. *J. Magn. Reson.*, **2009**, *200*, 296.

[24] Macchioni, A.; Ciancaleoni, G.; Zuccaccia, C.; Zuccaccia, D. Determining accurate molecular sizes in solution through NMR diffusion spectroscopy. *Chem. Soc. Rev.*, **2008**, *37*, 479.

[25] Chen, H. C.; Chen, S. H. Diffusion of crown ethers in alcohols. *J. Phys. Chem.*, **1984**, *88*, 5118.

[26] Huang, T. C., Toraya, H., Blanton, T. N.; Wu, Y. X-ray powder diffraction analysis of silver behenate, a possible low-angle diffraction standard. *J. Appl. Cryst.*, **1993**, *26*, 180.

[27] Kieffer J.; Karkoulis D. PyFAI, a versatile library for azimuthal regrouping. *J. Phys.: Conf. Ser.*, **2013**, *425*, 202012.

[28] App, J.; Konarev, V.; Volkov, V. V.; Sokolova, A. V.; Koch, M. H. J.; Svergun, D. I. PRIMUS: a Windows PC-based system for small-angle scattering data analysis. *J. Appl. Cryst.*, **2003**, *36*, 1277.

[29] Svergun, D. I. Determination of the regularization parameter in indirect-transform methods using perceptual criteria. *J. Appl Cryst.*, **1992**, *25*, 495.

[30] (a) Svergun, D. I. Restoring Low Resolution Structure of Biological Macromolecules from Solution Scattering Using Simulated Annealing. *Biophys J.*, **1999**, 2879. (b) Krebs, A.; Durchschlag, H.; Zipper, P. Small Angle X-Ray Scattering Studies and Modeling of Eudistylia vancouverii Chlorocruorin and Macrobdella decora Hemoglobin. *Biophys J.*, **2004**, *2*, 1173.

[31] te Velde, G.; Bickelhaupt, F. M.; Baerends, E. J.; Fonseca Guerra, C.; van Gisbergen, S. J. A.; Snijders, J. G. ; Ziegler, T. Chemistry with ADF. *J. Comput. Chem.*, **2001**, *22*, 931.

[32] Grimme, S.; Ehrlich, S.; Goerigk, L. Effect of the damping function in dispersion corrected density functional theory. *J. Comput. Chem.*, **2011**, *32*, 1456.

[33] van der Wijst, T.; Fonseca Guerra, C.; Swart, M.; Bickelhaupt, F. M.; Lippert, B. A Ditopic Ion-Pair Receptor Based on Stacked Nucleobase Quartets. *Angew. Chem. Int. Ed.*, **2009**, *48*, 3285.

[34] Klamt, A. Conductor-like Screening Model for Real Solvents: A New Approach to the Quantitative Calculation of Solvation Phenomena. *J. Phys. Chem.*, **1995**, *99*, 2224.

[35] Pye, C. C.; Ziegler, T. An implementation of the conductor-like screening model of solvation within the Amsterdam density functional package. *Theor. Chem. Acc.*, **1999**, *101*, 396.

[36] Swart, M.; Rösler, E.; Bickelhaupt, F. M. Proton Affinities in Water of Maingroup-Element Hydrides – Effects of Hydration and Methyl Substitution. *Eur. J. Inorg. Chem.*, **2007**, 3646.

[37] Riley, K. E.; Vondrasek, J.; Hobza, P. Performance of the DFT-D method, paired with the PCM implicit solvation model, for the computation of interaction energies of solvated complexes of biological interest. *Phys. Chem. Chem. Phys.*, **2007**, *9*, 5555.

[38] Jiang, T.; Lu, N.; Hang, Y.; Yang, J.; Mei, J.; Wang, J.; Hua, J.; Tian, H. Dimethoxy triarylamine-derived terpyridine–zinc complex: a fluorescence light-up sensor for citrate detection based on aggregation-induced emission. *J. Mater. Chem. C*, **2016**, *4*, 10040.

[39] Tatikonda, R.; Bhowmik, S.; Rissanen, K.; Haukka, M.; Cametti, M. Metallogel formation in aqueous DMSO by perfluoroalkyl decorated terpyridine ligands. *Dalton Trans.*, **2016**, 45, 12756.

[40] Wang, M.; Wang, K.; Wang, C.; Huang, M.; Hao, X.-Q. ; Shen, M.-Z.; Shi, G.-Q.; Zhang, Z.; Song, B.; Cisneros, A.; Song, M.-P.; Xu, B.; Li, X. Self-Assembly of Concentric Hexagons and Hierarchical Self-Assembly of Supramolecular Metal–Organic Nanoribbons at the Solid/Liquid Interface. *J. Am. Chem. Soc.*, **2016**, *138*, 9258.

[41] Cámara, V.; Barquero, N.; Bautista, D.; Gil-Rubio, J.; Vicente, J. Assembly of Heterometallic Rigid-Rod Complexes and Coordination Oligomers from Gold(I) Metalloligands. *Inorg. Chem.*, **2015**, *54*, 6147.

[42] Koshevoy, I.O.; Koskinen, L.; Smirnova, E.S.; Haukka, M.; Pakkanen, T. A.; Melnikov, A. S.; Tunik, S.P. Synthesis, structural characterization and luminescence studies of di- and trinuclear gold(I) alkynyl-phosphine complexes. *Z. Anorg. Allg. Chem.*, **2010**, *636*, 795.

[43] Castellano, S.; Günther, H.; Ebersole, S. Nuclear Magnetic Resonance Spectra of 2,2'-Bipyridyl. *J. Phys. Chem.*, **1965**, *69*, 4166.

[44] Gavara, R.; Aguiló, E.; Fonseca Guerra, C.; Rodríguez, L.; Lima, J.C. Thermodynamic Aspects of Aurophilic Hydrogelators. *Inorg. Chem*., **2015**, *54*, 5195.

[45] Shiotsuka, M.; Nishiko, N.; Keyaki, K.; Nozaki, K. Construction of a photoactive supramolecular system based on a platinum(II) bis-acetylide building block incorporated into a ruthenium(II) polypyridyl complex. *Dalton Trans.*, **2010**, *39*, 1831.

[46] Xu, H. B.; Zhang, L. Y.; Ni, J.; Chao, H. Y.; Chen, Z. N. Conformation Changes and Luminescent Properties of Au-Ln (Ln = Nd, Eu, Er, Yb) Arrays with 5-Ethynyl-2,2′-Bipyridine. *Inorg. Chem*., **2008**, *47*, 10744.

[47] Rodríguez, L.; Ferrer, M.; Crehuet, R.; Anglada, J.; Lima, J.C. Correlation between Photophysical Parameters and Gold–Gold Distances in Gold(I) (4-Pyridyl)ethynyl Complexes. *Inorg. Chem*. **2012**, *51*, 7636.

[48] Pazderski, L.; Pawlak, T.; Sitkowski, J.; Kozerski, L.; Szlyk, E. 1H NMR assignment corrections and 1H, 13C, 15N NMR coordination shifts structural correlations in Fe(II), Ru(II) and Os(II) cationic complexes with 2,2′-bipyridine and 1,10-phenanthroline. *Magn. Reson. Chem.*, **2010**, *48*, 450.

Table of Contents (TOC)

Reversible self-assembly of water soluble gold(I) complexes

Elisabet Aguiló, Artur J. Moro, Raquel Gavara, Ignacio Alfonso, Yolanda Pérez, Francesco Zaccaria, Célia Fonseca Guerra, Marc Malfois, Clara Baucells, Montserrat Ferrer, João Carlos Lima and Laura Rodríguez.